

# Analysis of $\lambda = 6$ cm VLBI polarization observations of a complete sample of northern BL Lacertae Objects

D. C. Gabuzda<sup>1,2</sup>, A. B. Pushkarev<sup>2</sup> and T. V. Cawthorne.<sup>3</sup>

<sup>1</sup>*Joint Institute for VLBI in Europe, Postbus 2, 7990 AA Dwingeloo, The Netherlands*

<sup>2</sup>*Astro Space Centre, P.N. Lebedev Physical Institute, Leninsky Prospekt 53, 117924 Moscow, Russia.*

<sup>3</sup>*Department of Physics and Astronomy, University of Central Lancashire, Preston, Lancashire, PR1 2HE.*

2 October 2018

## ABSTRACT

The results of VLBI total intensity ( $I$ ) and linear polarization ( $P$ ) observations at  $\lambda = 6$  cm are presented for ten radio bright BL Lacertae objects. These images complete first-epoch polarization observations for the 1-Jy sample of northern BL Lacertae objects defined by Kühr and Schmidt. Estimates of superluminal speeds are presented for several sources, bringing the total number of sources in the sample for which such estimates are available to 16. Second epoch observations currently being reduced should yield speed estimates for VLBI features in essentially all the sources in the sample. The jet magnetic fields of these BL Lacertae objects are usually transverse to the local jet direction, but a sizeable minority (about 30%) have VLBI jet components with longitudinal magnetic fields. This may suggest that the conditions in the VLBI jets of BL Lacertae objects are favorable for the formation of relativistic shocks; alternatively, it may be that the toroidal component of the intrinsic jet magnetic field is characteristically dominant in these sources.

**Key words:** BL Lacertae objects: general – BL Lacertae objects: individual: (0003–066, 0814+425, 0820+225, 0823+033, 1334–127, 1732+389, 2131–021, 2150+173, 2155–152, 2254+074 – polarization — radio sources: galaxies

## 1 INTRODUCTION

BL Lacertae objects are active galactic nuclei whose most characteristic distinguishing property is their relatively low-luminosity optical line emission; in many cases, their optical continua are completely featureless. Like many high-polarization quasars, BL Lacertae objects have strong and variable polarization in wavebands ranging from optical through radio; they usually have compact, flat-spectrum radio structure, and point-like optical structure. For some, luminous elliptical host galaxies are observed (Angel and Stockman 1980; Miller 1981; Kollgaard 1994), though the optical images of many BL Lacertae objects remain unresolved, even in high-resolution observations (e.g. Falomo 1996). The radio emission and much of the optical emission is believed to be synchrotron radiation. Historically, BL Lacertae objects were first detected primarily via radio surveys, and strong radio emission was earlier thought to be characteristic of this type of AGN. More recently, large numbers of BL Lacertae objects with much weaker radio emission have been discovered by X-ray surveys. The relationship between these so-called “radio” and X-ray” BL Lacertae objects is not entirely clear; the most popular cur-

rent hypotheses are (1) that they are similar objects whose spectral energy distributions peak in the infrared and X-ray, respectively, with the radio emission in radio BL Lacertae objects experiencing a larger intrinsic relativistic enhancement (Giommi & Padovani 1994; Padovani & Giommi 1995; Fossati et al. 1997), and (2) that they are intrinsically identical objects whose jets are oriented at different characteristic angles to the line of sight, with X-ray BL Lacertae objects being viewed further “off-axis” (Stocke et al. 1985; Maraschi et al. 1986). In the broader context of unified schemes, it is usually thought that the “parent population” of BL Lacertae objects is primarily FR I radio galaxies (Browne 1983; Wardle, Moore & Angel 1984).

Previous VLBI polarization observations of radio BL Lacertae objects at 6 cm and 3.6 cm (Gabuzda & Cawthorne 1996, Gabuzda et al. 1999, and references therein) have revealed a tendency for the electric vector  $\chi$  in polarized knots in the VLBI jets to lie nearly along the local jet direction. The degrees of polarization in the jet components of BL Lacertae objects have been observed to be as high as  $m \sim 60 - 70\%$ , with typical values  $m \sim 5 - 15\%$ , indicating that these components are optically thin and that in at least some cases the magnetic field is very highly or-

**Table 1.** ANTENNAS USED

Antenna	Diameter (m)	$T_{sys,R}$ (K)	$T_{sys,L}$ (K)	$g$ (K/Jy)	Epoch
Medicina	32	60	50	0.160	1, 2
Effelsberg	100	60	50	0.991	1, 2
WSRT	$\sqrt{14} \times 25$	120	120		2
St. Croix	25	45	35	0.102	2
Hancock	25	55	60	0.092	2
Haystack	37	75	65	0.130	1
Green Bank	43	35	40	0.227	1, 2
North Liberty	25	45	45	0.120	1, 2
Phased VLA	$\sqrt{27} \times 25$	**	**	**	1
Kitt Peak	25	65	65	0.120	1
Owens Valle	25	110	110	0.120	1, 2
Brewster	25	35	35	0.088	2
Mauna Kea	25	35	35	0.090	2

Epochs: 1 = 1992.23; 2 = 1995.41

dered. Assuming the jet components to be optically thin, the observed typical  $\chi$  orientation implies that the associated magnetic fields are perpendicular to the direction of the jet. One natural interpretation of this transverse magnetic field structure is that the visible jet components are associated with relativistic shocks that compress an initially tangled magnetic field, enhancing the magnetic field transverse to the compression (Laing 1980; Hughes, Aller and Aller 1989). As images for more BL Lacertae objects have become available, it has become increasingly clear that there are also a sizeable minority of these sources in which, in contrast, longitudinal magnetic fields dominate in at least some parts of their VLBI jets.

At 6 cm, the degrees of polarization of the cores of BL Lacertae objects ( $\sim 2 - 9\%$ ) are, on average, higher than those of quasars ( $\leq 2\%$ ). Recent 6 cm space VLBI polarization observations of the BL Lacertae object 1803+784 (Gabuzda 1999) indicate that this is due to the fact that the observed core polarizations include a substantial contribution from newly emerging knots, as suggested by Gabuzda et al. (1994b). Previous observations have shown the distribution of core  $\chi$  orientations at 6 cm to be bimodal, with  $\chi$  either aligned with or transverse to the inner jet direction; there is some evidence that  $\chi_{core}$  is roughly perpendicular to the jet when the cores are quiescent, and aligns with the jet at epochs when emission from newly emerging shock components dominate the observed “core” polarization (Gabuzda et al. 1994b, Gabuzda & Cawthorne 1996).

To elucidate the nature of the characteristic VLBI total intensity ( $I$ ) and polarization ( $P$ ) structures observed for radio-bright BL Lacertae objects, we are engaged in an ongoing project to obtain multi-epoch, multi-frequency VLBI  $I$  and  $P$  images for all sources in the complete sample of BL Lacertae objects defined by Kühr and Schmidt (1990). These sources have 6 cm fluxes of at least 1 Jy, radio spectral indices  $\alpha \geq -0.5$  ( $S_\nu \sim \nu^{+\alpha}$ ), rest frame equivalent widths of the strongest emission lines less than 5 Å, and optical counterparts on the Palomar Sky Survey plates with brightness greater than  $20^m$ . VLBI  $I$  and  $P$  images for most of the sample sources are presented by Roberts, Gabuzda & Wardle (1987); Gabuzda, Roberts & Wardle (1989b); Gabuzda

**Table 2.** INTEGRATED ROTATION MEASURES

Source	RM (rad/m <sup>2</sup> )	RM Ref	Rot. at $\lambda 6$ cm (deg)
0003–066	+13	2	+3
0814+425	+23	1	+5
0820+225	+81	2	+17
0823+033	1	2	+1
1334–127	–23	2	–5
1732+389	+67	2	+14
2131–021	+46	2	+9
2150+173	–39	2	–8
2155–152	+19	2	+4
2254+074	–30	2	–6

References: 1 = Rusk 1988;  
2 = Gabuzda and Pushkarev, in preparation.

et al. (1992, 1994b); and Gabuzda, Pushkarev & Cawthorne (1999). The ten sets of  $I$  and  $P$  images presented here complete our first-epoch images for the 34 sources in the original sample (one, 1334–127, was subsequently reclassified as a quasar, so that the final number of sources in the complete BL Lac sample is 33). These are the first  $P$  images for these ten sources, and in a number of cases, the first 6 cm  $I$  images as well.

## 2 OBSERVATIONS

The observations of all sources except 0003–066 were made in March 1992 (1992.23), using an 8-element global VLBI array. The observations for 0003–066 were made in May 1995 (1995.41) using a 10-element global array. The antennas used in both experiments are listed in Table 1. The observations were made under the auspices of the US and European VLBI networks. The data were recorded using the MkIII system, and the data were subsequently correlated using the Mk IIIA correlators at Haystack Observatory (1992.23) and the Max-Planck-Institut-für-Radioastronomie in Bonn (1995.41).

The polarization calibration of these data was performed as described by Roberts, Wardle and Brown (1994). The instrumental polarizations (“D-terms”) were determined using observations of the unpolarized sources 3C84 and OQ208; the overall D-terms residuals are at a level  $\simeq 0.5\%$ . The VLBI polarization position angles were calibrated by comparing the total VLBI-scale and VLA core polarizations for the especially compact and relatively strongly polarized sources 0823+033 and 1749+096. The rotations required to align  $\chi$  for the total VLBI-scale polarizations of these sources with  $\chi$  for their VLA core polarizations agreed to within less than one degree, suggesting that the overall VLBI polarization position angle calibration is good to about this level of precision.

Images of the distribution of total intensity  $I$  were made using a self-calibration algorithm similar to that described by Cornwell and Wilkinson (1981). Maps of the linear polarization<sup>\*</sup>  $P$  were made by referencing the cal-

<sup>\*</sup>  $P = pe^{2i\chi} = mIe^{2i\chi}$ , where  $p = mI$  is the polarized intensity,  $m$  is the fractional linear polarization, and  $\chi$  is the position angle

ibrated cross-hand fringes to the parallel-hand fringes using the antenna gains determined in the hybrid mapping, Fourier transforming the cross-hand fringes, and performing a complex CLEAN. One byproduct of this procedure is to register the  $I$  and  $P$  maps to within a small fraction of a beamwidth, so that corresponding  $I$  and  $P$  images may be directly superimposed.

### 3 RESULTS

Results for the ten sources are discussed below. In each of the images, the restoring beams are shown as crosses in a corner of the images. For the linear polarization maps, the contours are those of polarized intensity  $p$ , and the plane of the electric vector is indicated by the polarization position angle vectors that are superimposed.

There is always the possibility that the observed polarization position angles include some contribution due to Faraday rotation along the line of sight to the emission region. Multi-frequency VLBI studies of a number of quasars have revealed the presence of non-uniform rotation-measure distributions on parsec scales in some sources (Taylor 1998, 2000; Nan et al. 1999). At the same time, other sources show no clear evidence for substantial local (non-Galactic) rotation measures (Gabuzda & Gómez 2000). In the absence of simultaneous multi-wavelength VLBI polarimetry, the only Faraday correction that may be applied is one based on integrated measurements. For reference, the rotation measures for the ten sources considered here are summarized in Table 2. All the rotations produced at  $\lambda = 6\text{cm}$  by the integrated rotation measures in Table 2 are less than about  $15^\circ$ ; all except that for 1732+389 and 0820+225 are less than  $10^\circ$  (Table 2). Therefore, application of these rotations is probably unlikely to introduce large errors in the resulting  $\chi$  values. The  $\chi$  values for all sources except for 0820+225 have accordingly been corrected using the rotation measures in Table 2; the possibility of offsets in  $\chi$  due to local rotation measures that have not been accounted for should be borne in mind, however. The case of 0820+225 is discussed below: for this source, quasi-simultaneous multi-frequency VLBA polarization images (Gabuzda, Pushkarev & Garnich, in prep.) have revealed a non-uniform rotation-measure distribution on milliarcsecond scales, so that it is clearly not appropriate to apply the integrated rotation measure to each of the VLBI components.

Models for the source structures were derived by fitting the complex  $I$  and  $P$  visibilities that come from the hybrid mapping process as described by Roberts, Gabuzda and Wardle (1987) and Gabuzda, Wardle and Roberts (1989b). The model fits are shown in Table 3. We denote distance from the core by  $r$  and the VLBI jet direction by  $\theta$ . In all cases, we checked for consistency between the model-fitting results, the distribution of CLEAN components, and the visual appearance of the images. We included components in the models only if there was clear evidence for them in the CLEAN components derived during the imaging process.

The  $I$  and  $P$  visibilities were fit separately, in order to allow for small differences in the positions and sizes of

of the electric vector on the sky, measured from north through east.

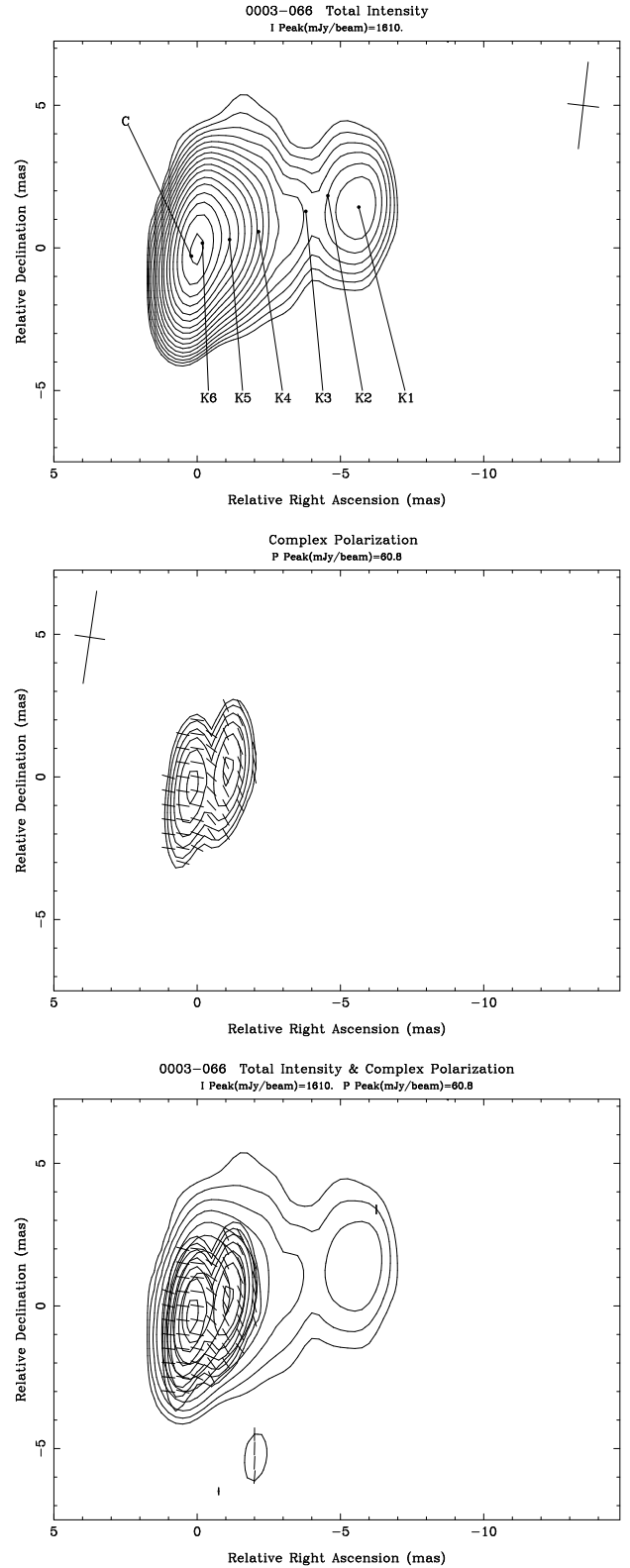


**Figure 1.** VLBI hybrid maps of 0003-066: (a) Total intensity, with contours at  $-0.5, 0.5, 0.7, 1.0, 1.4, 2.0, 2.8, 4.0, 5.6, 8.0, 11, 16, 23, 32, 45, 64$ , and 90% of the peak brightness of  $1.61\text{ Jy/beam}$ . (b) Linear polarization, with contours of polarized intensity at  $16, 23, 32, 45, 64$ , and 90% of the peak brightness of  $61\text{ mJy/beam}$ , and  $\chi$  vectors superimposed. (c) Superposition of  $P$  image (heavy lines) over the  $I$  image, with every other  $I$  contour omitted.

**Table 3.** SOURCE MODELS

	$I$ (mJy)	$p$ (mJy)	$\chi_0^a$ (deg)	$m$ (%)	$r$ (mas)	$\Delta r$ (mas)	$\theta$ (deg)	$\Delta\theta$ (deg)	FWHM (mas)
0003–066									
C	922	63.3	79	6.8	–	–	–	–	0.25
K6	824	< 10	–	< 1.2	0.60	–	–40	–	0.23
K5	372	55.8	21	13.6	1.46	–	–67	–	0.46
K4	150	< 10	–	< 7	2.51	–	–70	–	1.94
K3	11	< 10	–	< 7	4.31	–	–68	–	0.02
K2	15	< 10	–	< 38	5.23	–	–66	–	0.33
K1	97	< 10	–	< 11	6.10	–	–74	–	1.15
0814+425									
C	620	< 3	–	< 0.5	–	–	–	–	0.48
K5	200	22.2	26	11.1	0.99	0.01	128	1	0.50
K4	35	9.2	84	26.2	2.29	0.02	111	1	0.92
K3	11	< 3	–	< 27	3.56	0.03	108	1	0.74
K2	19	< 3	–	< 16	4.89	0.07	101	2	1.48
K1	10	< 3	–	< 30	6.34	0.13	106	2	1.08
0820+225									
C	198	< 3	–	< 1.5	–	–	–	–	0.20
K11	119	7.4	–26	6.2	2.16	0.07	–173	1	0.80
K10	43	8.0	–69	18.6	4.26	0.17	–167	1	1.03
K9	47	< 3	–	< 6.4	5.84	0.13	–156	1	1.51
K8	68	12.2	16	17.9	8.86	0.09	–133	1	2.28
K7	22	9.2	–5	41.8	11.33	0.16	–132	1	1.52
K6	113	7.2	–16	6.4	12.84	0.07	–130	1	2.95
K5	90	20.8	–29	23.1	17.45	0.08	–132	1	2.87
K4	13	< 3	–	< 23	19.99	0.10	–136	1	0.24
K3	165	24.1	–70	14.6	21.70	0.06	–135	1	1.76
K2	60	9.7	–80	16.2	23.38	0.08	–132	1	1.27
K1	180	< 3	–	< 1.7	24.81	0.07	–138	1	2.69
0823+033									
C	1494	60.6	–13	4.0	–	–	–	–	0.07
K3	415	< 15	–	< 3.6	0.71	0.03	30	3	0.18
K2	29	< 15	–	< 52	3.16	0.31	31	4	0.47
K1	25	< 15	–	< 60	4.81	0.23	28	2	0.23
1334–127*									
C	3822	67.0	83	1.8	–	–	–	–	0.14
K3	201	37.7	54	18.8	2.25	0.06	147	1	0.20
K2	56	< 11	–	< 20	2.26	0.14	110	9	0.01
K1	26	< 11	–	< 42	7.18	0.23	120	3	0.20
1732+389									
C	923	18.7	5	2.0	–	–	–	–	0.32
K3	116	8.0	33	6.8	0.80	0.07	103	7	0.08
K2	21	< 4	–	< 19	2.48	0.30	112	3	0.15
K1	10	< 4	–	< 40	3.67	0.19	108	5	0.66
2131–021†									
C	1011	18.8–22.5	–(28–13)	1.8–2.2	–	–	–	–	0.11
K5	344	< 6	–	< 1.7	0.41	0.03	100	6	0.13
K4	19	< 6	–	< 32	1.77	0.30	70	25	0.14
K3	18	< 6	–	< 33	2.82	0.09	75	6	0.14
K2	12	< 6	–	< 50	5.39	0.09	86	10	0.14
K1	17	< 6	–	< 35	6.58	0.04	88	3	0.12
2155–152†									
C	207	21.4–46.9	52.0	10.3–22.6	–	–	–	–	0.16
K	844	< 8	–	< 1.0	1.55	0.04	–144	1	0.28
K	897	49.3	–76.2	5.5	4.52	0.05	–161	1	1.50
K1	39	< 8	–	< 20	9.41	0.20	–146	1	0.05

<sup>a</sup> Observed  $\chi$  values for all sources except for 0820+225 corrected using integrated rotation measures in Table 2 (see text).

\* The VLA and VLBI polarizations were variable during the VLBI run; the indicated  $p$  and  $\chi$  correspond to one two-hour interval during the run (see text).

† The VLA and VLBI polarizations were variable during the VLBI run; the indicated  $p$  and  $\chi$  give the ranges covered during the VLBI run.

**Table 3.** SOURCE MODELS (CONT'D)

	$I$ (mJy)	$p$ (mJy)	$\chi_0^a$ (deg)	$m$ (%)	$r$ (mas)	$\Delta r$ (mas)	$\theta$ (deg)	$\Delta\theta$ (deg)	FWHM (mas)
2150+173									
C	222	11.5	−7	5.2	—	—	—	—	0.13
K5	137	3.2	−23	2.3	0.76	0.02	−96	3	0.79
K4	26	< 2	—	< 8	1.51	0.10	−74	5	0.47
K3	35	4.5	−4	12.8	3.03	0.05	−85	3	1.86
K2	40	< 2	—	< 5	5.73	0.03	−81	1	0.85
K1	45	2.7	52	6.0	6.51	0.03	−83	1	1.01
2254+074									
C	104	< 9	—	< 9	—	—	—	—	0.25
K3	20	< 9	—	< 45	0.85	0.04	−84	9	0.34
K2	25	< 9	—	< 36	2.70	0.06	−110	3	1.34
K1	7	< 9	—	< 100	3.69	0.30	−127	6	0.55

<sup>a</sup> Observed  $\chi$  values for all sources except for 0820+225 corrected using integrated rotation measures in Table 2 (see text).

corresponding  $I$  and  $P$  components, either intrinsic to the source structure or associated with residual calibration errors. When  $P$  components have been identified with specific  $I$  components, the two positions agree to within their  $3\sigma$  errors. When calculating the degrees of polarization  $m$  for individual features, we have not taken into account possible small physical offsets between the corresponding  $I$  and  $P$  components, so that the  $m$  values in Table 3 represent averages for each component.

The errors of the separations of jet components from the core given in Table 3 are formal  $1\sigma$  errors, corresponding to an increase in the best-fit  $\chi^2$  by unity. The smallest of these formal errors almost certainly underestimate the actual errors; realistically, the smallest  $1\sigma$  errors in component separations are probably no less than  $\sim 0.05$  mas.

In our 1992.23 VLBI run, the polarizations of three of the eighteen sources—1334−127, 2131−021, and 2155−152—varied during the VLBI observations. We were able to detect these variations since the phased VLA was included in the VLB array, so that we had measurements of the integrated total intensity and polarization during each of the VLBI scans. Summary information about the polarizations of these sources is given below; the polarization variations are analysed in detail in an accompanying paper by Gabuzda et al. (2000).

We assume throughout a Friedmann universe with Hubble constant of  $100h$  km sec<sup>−1</sup> Mpc<sup>−1</sup> and  $q_0 = 0.5$ .

### 3.1 0003−066

The source 0003−066 has a redshift of  $z = 0.35$ . The 2 cm image of Kellermann et al. (1998) and 13 and 4 cm images of Fey & Charlot (1997) show a jet extending toward the northwest. Our  $I$  image (Fig. 1) clearly shows the straight jet in position angle  $\theta = -75^\circ$ , in which we have modelled six components (Fig. 1). The linear polarization map shows a double structure, where one component corresponds to the core and the other to the jet feature K5. The polarization position angle  $\chi$  in the jet is nearly perpendicular to the jet axis.

### 3.2 0814+425

Observations by Wills & Wills (1976) provided evidence that the redshift of this object is  $z = 0.258$ . Subsequent observations (Stickel et al. 1993a) have not directly confirmed this value, though the CFHT observations of Wurtz et al. (1996) showed the host galaxy to be resolved, consistent with a redshift of 0.258. The 2 cm image of Kellermann et al. (1998) for epoch 1995 April shows a jet that emerges to the east, then appears to bend sharply to the south. Our 6 cm images (Fig. 2) suggest a more gently curving jet structure that initially emerges in position angle  $\sim 130^\circ$ , then turns more nearly east. Our images do not show clear evidence for the sharp bending observed by Kellermann et al. (1998), even in the innermost part of the jet. VLBA images for epoch 1997 February at 2, 4, and 6 cm currently being analyzed (Pushkarev et al., in prep.) clearly show the predominant jet direction to be nearly due east, with the 2 cm image in good qualitative agreement with that of Kellermann et al. (1998). This suggests that the compact eastern extension in the 2 cm images referred to above may have emerged after the 6 cm observations presented here. We detect polarization in the two innermost jet components in our images;  $\chi$  appears to be transverse to the local jet direction in K5 and aligned with the local jet direction in K4.

### 3.3 0820+225

The redshift of this source is  $z = 0.95$  (Stickel et al. 1993a), making it one of the most distant objects in the sample. As far as we are aware, ours are the first VLBI images of this source. It displays a rather extraordinary VLBI jet, with very rich  $I$  and  $P$  structure. There is much more extended emission than observed in most of the sample objects; this is particularly striking given its large redshift. The jet extends nearly 30 mas to the southwest, and only a small fraction of the total flux in the VLBI image is contained in the VLBI core. We have modelled the image as a core plus 11 jet components. We expect that this is a good description of the source within 15–20 mas from the core, but our jet components K1–K4 represent only an approximate model for the bright, extended region at the end of the visible jet. The

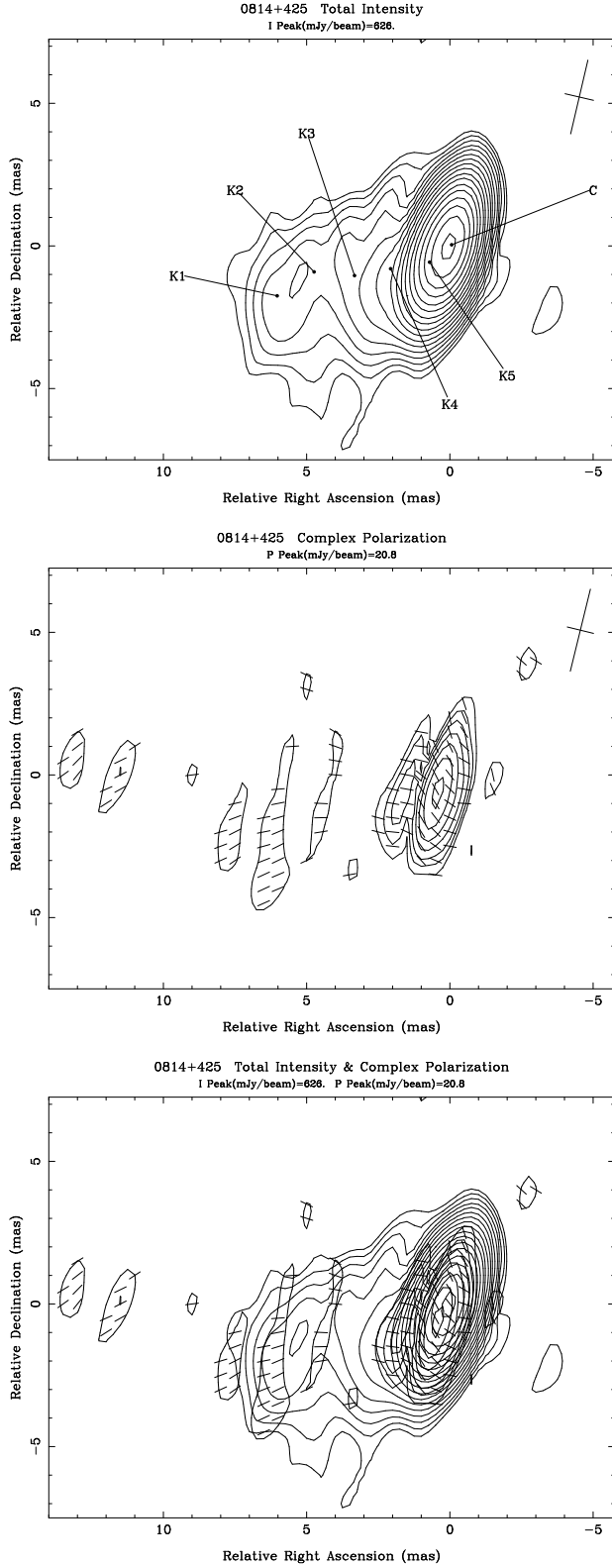


**Figure 2.** Total intensity VLBI hybrid map of 0814+425, with contours at  $-0.3, 0.3, 0.5, 0.7, 1.0, 1.4, 2.0, 2.8, 4.0, 5.6, 8.0, 11, 16, 23, 32, 45, 64$ , and 90% of the peak brightness of  $0.63 \text{ Jy/beam}$ . (b) Linear polarization, with contours of polarized intensity at  $11, 16, 23, 32, 45, 64$ , and 90% of the peak brightness of  $21 \text{ mJy/beam}$ , and  $\chi$  vectors superimposed. (c) Superposition of  $P$  image (heavy lines) over the  $I$  image, with every other  $I$  contour omitted.

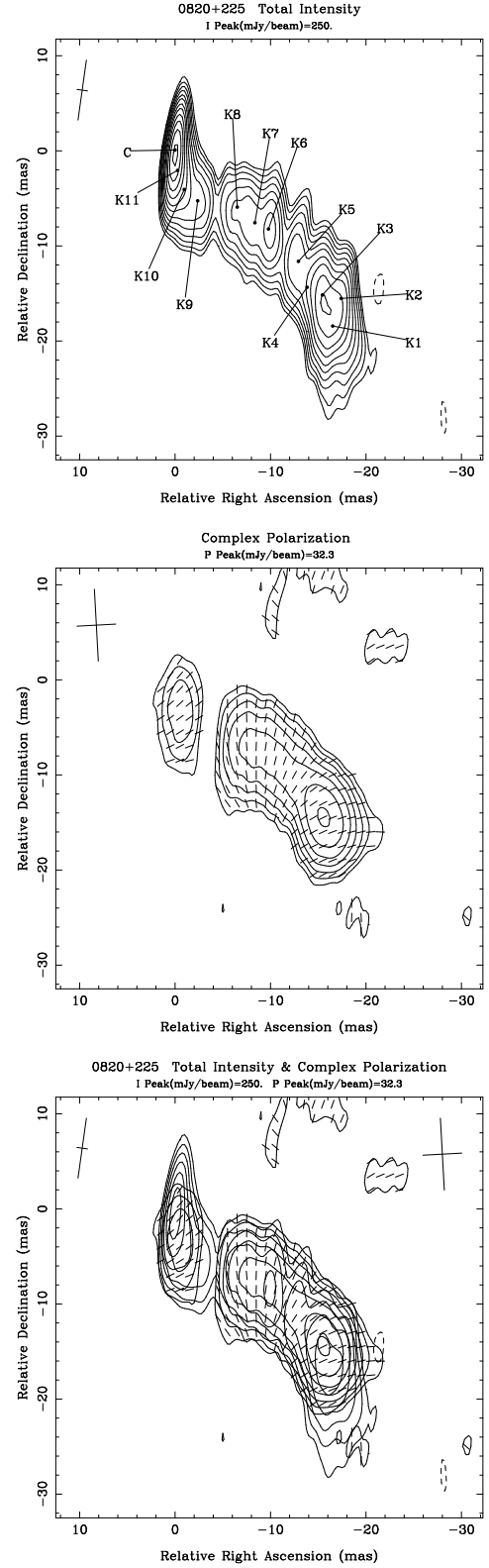


**Figure 3.** Total intensity VLBI hybrid map of 0820+225, with contours at  $-2.0, 2.0, 2.8, 4.0, 5.6, 8.0, 11, 16, 23, 32, 45, 64$ , and 90% of the peak brightness of  $0.25 \text{ Jy/beam}$ . (b) Linear polarization, with contours of polarized intensity at  $12, 17, 24, 34, 48, 68$ , and 96% of the peak brightness of  $32 \text{ mJy/beam}$ , and  $\chi$  vectors superimposed. (c) Superposition of  $P$  image (heavy lines) over the  $I$  image, with every other  $I$  contour omitted.

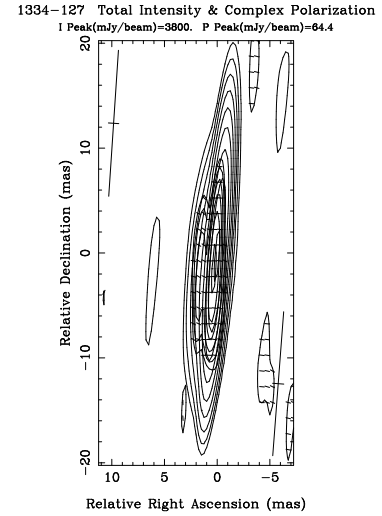
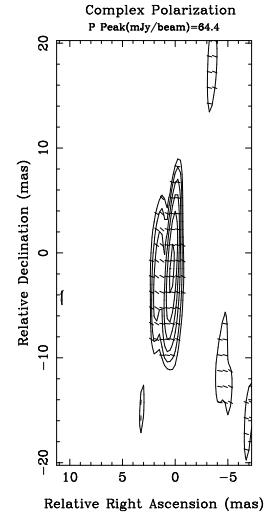
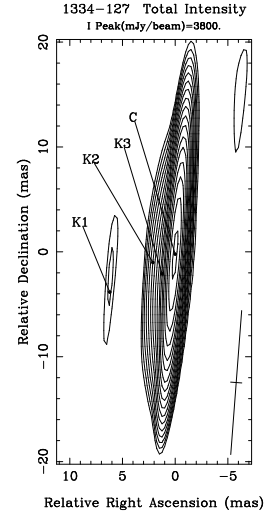
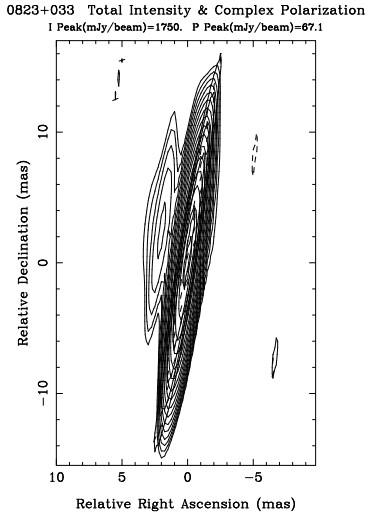
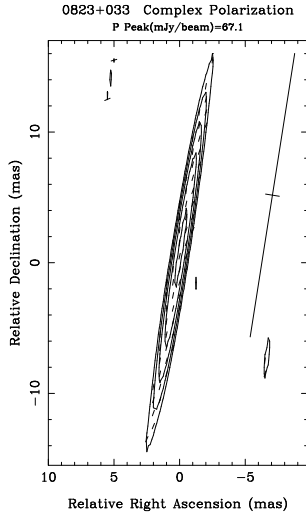
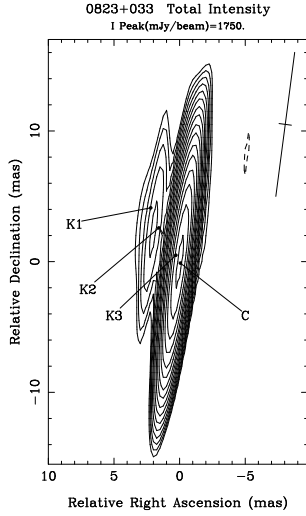


**Figure 4.** Total intensity VLBI hybrid map of 0823 + 033, with contours at  $-0.5, 0.5, 0.7, 1.0, 1.4, 2.0, 2.8, 4.0, 5.6, 8.0, 11, 16, 23, 32, 45, 64$ , and 90% of the peak brightness of 1.75 Jy/beam. (b) Linear polarization, with contours of polarized intensity at 23, 32, 45, 64, and 90% of the peak brightness of 67 mJy/beam, and  $\chi$  vectors superimposed. (c) Superposition of  $P$  image (heavy lines) over the  $I$  image, with every other  $I$  contour omitted.

**Figure 5.** Total intensity VLBI hybrid map of 1334 – 127, with contours at  $-0.35, 0.5, 0.7, 1.0, 1.4, 2.0, 2.8, 4.0, 5.6, 8.0, 11, 16, 23, 32, 45, 64$ , and 90% of the peak brightness of 3.80 Jy/beam. (b) Linear polarization, with contours of polarized intensity at 17, 24, 34, 48, 68, and 96% of the peak brightness of 64 mJy/beam, and  $\chi$  vectors superimposed. (c) Superposition of  $P$  image (heavy lines) over the  $I$  image, with every other  $I$  contour omitted.

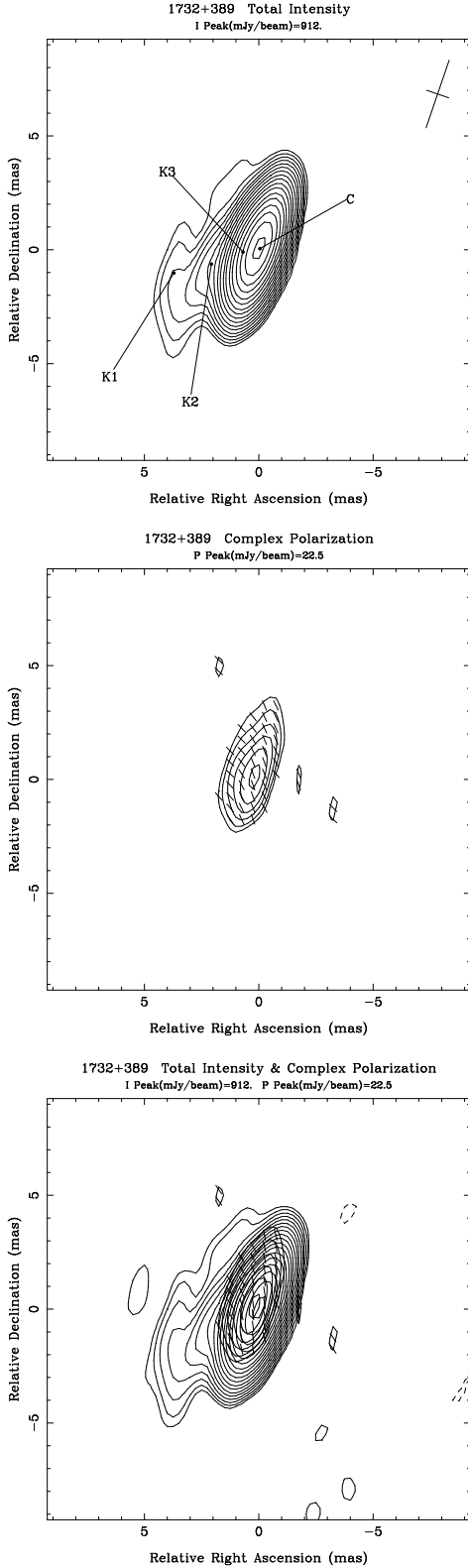


**Figure 6.** Total intensity VLBI hybrid map of 1732+389, with contours at  $-0.35, 0.35, 0.5, 0.7, 1.0, 1.4, 2.0, 2.8, 4.0, 5.6, 8.0, 11, 16, 23, 32, 45, 64$ , and 90% of the peak brightness of  $0.91 \text{ Jy/beam}$ . (b) Linear polarization, with contours of polarized intensity at  $16, 23, 32, 45, 64$ , and 90% of the peak brightness of  $22 \text{ mJy/beam}$ , and  $\chi$  vectors superimposed. (c) Superposition of  $P$  image (heavy lines) over the  $I$  image, with every other  $I$  contour omitted.

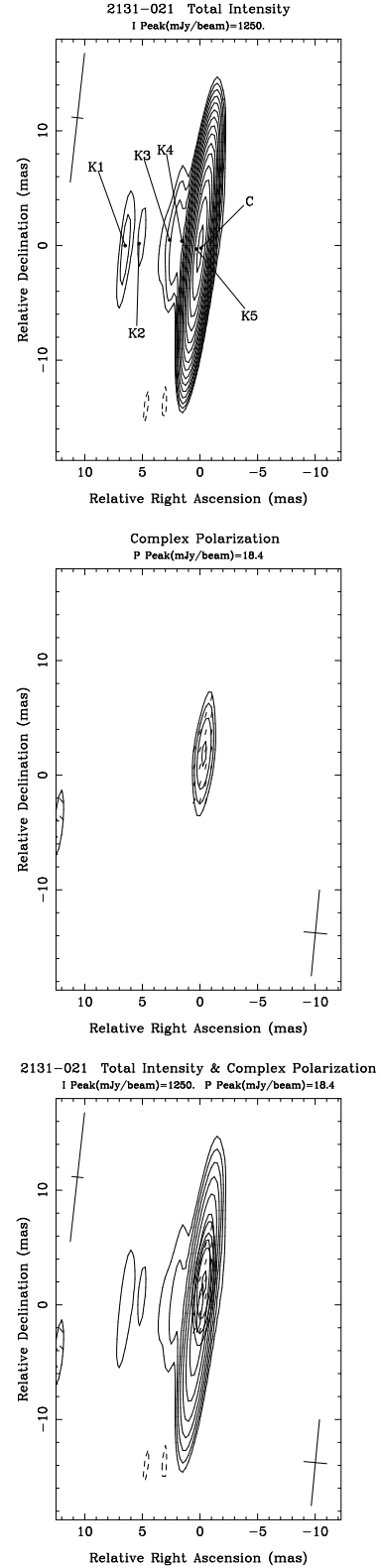


**Figure 7.** Total intensity VLBI hybrid map of 2131-021, with contours at  $-0.5, 0.5, 0.7, 1.0, 1.4, 2.0, 2.8, 4.0, 5.6, 8.0, 11, 16, 23, 32, 45, 64$ , and 90% of the peak brightness of  $0.95 \text{ Jy/beam}$ . (b) Linear polarization, with contours of polarized intensity at  $34, 48, 68$ , and 96% of the peak brightness of  $18 \text{ mJy/beam}$ , and  $\chi$  vectors superimposed. (c) Superposition of  $P$  image (heavy lines) over the  $I$  image, with every other  $I$  contour omitted.



observed orientation of  $\chi$  is transverse to the jet; however, multi-frequency VLBI polarization observations (Gabuzda and Pushkarev, in preparation) indicate the presence of a large local rotation measure in the inner jet (near K10), and the derotated  $\chi$  values in this region are well aligned with the local jet direction.

### 3.4 0823+033

The redshift of this source is  $z = 0.506$  (Stickel et al. 1993a). The 2 cm image of Kellermann et al. (1998) and 13 and 4 cm images of Fey & Charlot (1997) show a jet extending to the northeast. The relatively weak jet is also visible in our images (Fig. 4); we detected polarization only from the VLBI core.

### 3.5 1334-127

This extremely bright and compact source has a redshift of  $z = 0.54$  (Wilkes 1986; Stickel et al. 1993b). Though this source was included in the Kühr & Schmidt (1990) BL Lac sample, it was subsequently reclassified as a quasar by Stickel et al. (1993b). The 2 cm image of Kellermann et al. (1998) shows a jet toward the southeast. The dominant orientation for the inner VLBI jet in our image is  $\theta \sim 150^\circ$ . The polarization of this source varied during the VLBI observations. The  $P$  map in Fig. 5b was obtained for the time subinterval considered in the intraday variability analysis (Gabuzda et al. 2000) that had the best  $u - v$  coverage. The polarization position angle  $\chi$  in the brightest jet component is roughly perpendicular to the inner-jet direction. The orientation of  $\chi$  in the core relative to the jet direction is not clear; it is interesting, however, that this orientation is nearly the same as that observed by Lister et al. (1998) in the inner VLBI jet at 7 mm (where it is also oblique), suggestive that our 6 cm “core” emission may be associated with this same region. The 6 cm jet is fairly highly polarized,  $\sim 18\%$ .

### 3.6 1732+389

The redshift of this object is  $z = 0.976$ , making it one of the most distant sources in the sample. The 6 cm VLBI image of Xu et al. (1995) showed a compact VLBI jet toward the east. Our images (Fig. 6) show the jet more clearly. The jet contains three components, with polarization detected in the core and innermost jet component K3. The  $\chi$  in K3 is roughly perpendicular to the jet direction.

### 3.7 2131-021

This source has the largest redshift among the sample objects,  $z = 1.28$  (Drinkwater et al. 1997). The structure is very compact, with a jet extending nearly directly east (Fig. 7); the faint jet is also visible in the 2 cm image of Kellermann et al. (1998) and the 13 and 4 cm images of Fey & Charlot (1997). We detected polarization only in the VLBI core, and this polarization varied during the VLBI observations. The  $P$  map in Fig. 7b was obtained for one time subinterval considered in the intraday variability analysis (Gabuzda et al. 2000). The degree of polarization was only

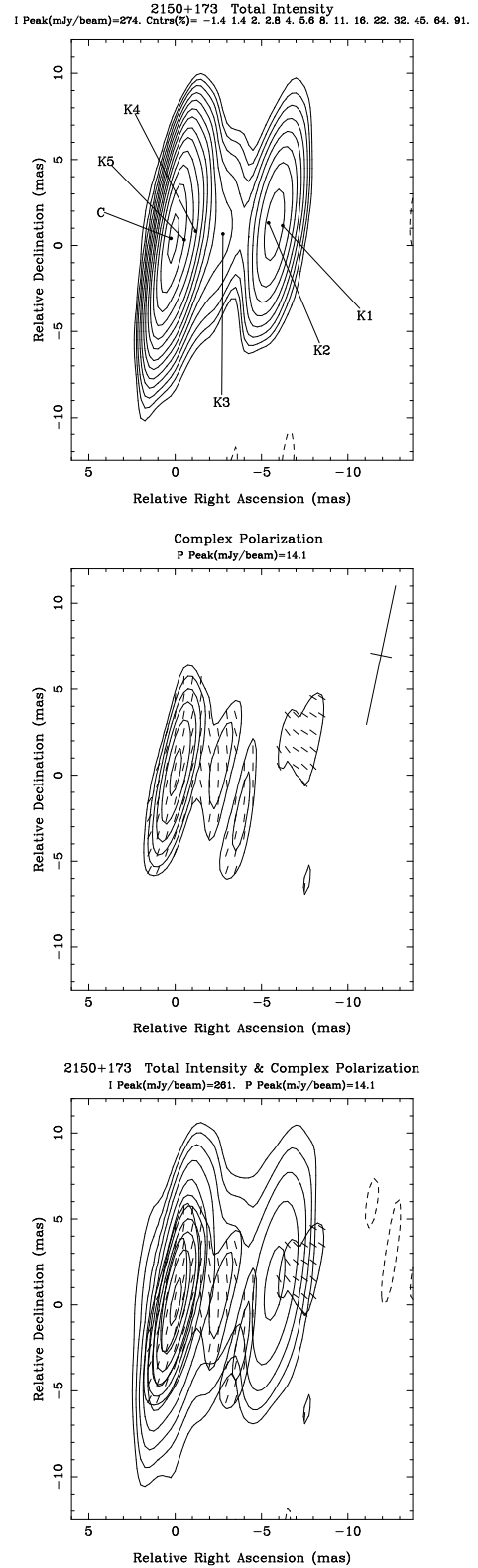


**Figure 8.** Total intensity VLBI hybrid map of 2150+173, with contours at  $-1.4, 1.4, 2.0, 2.8, 4.0, 5.6, 8.0, 11, 16, 23, 32, 45, 64$ , and  $90\%$  of the peak brightness of  $0.27$  Jy/beam. (b) Linear polarization, with contours of polarized intensity at  $16, 23, 32, 45, 64$ , and  $90\%$  of the peak brightness of  $14$  mJy/beam, and  $\chi$  vectors superimposed. (c) Superposition of  $P$  image (heavy lines) over the  $I$  image, with every other  $I$  contour omitted.

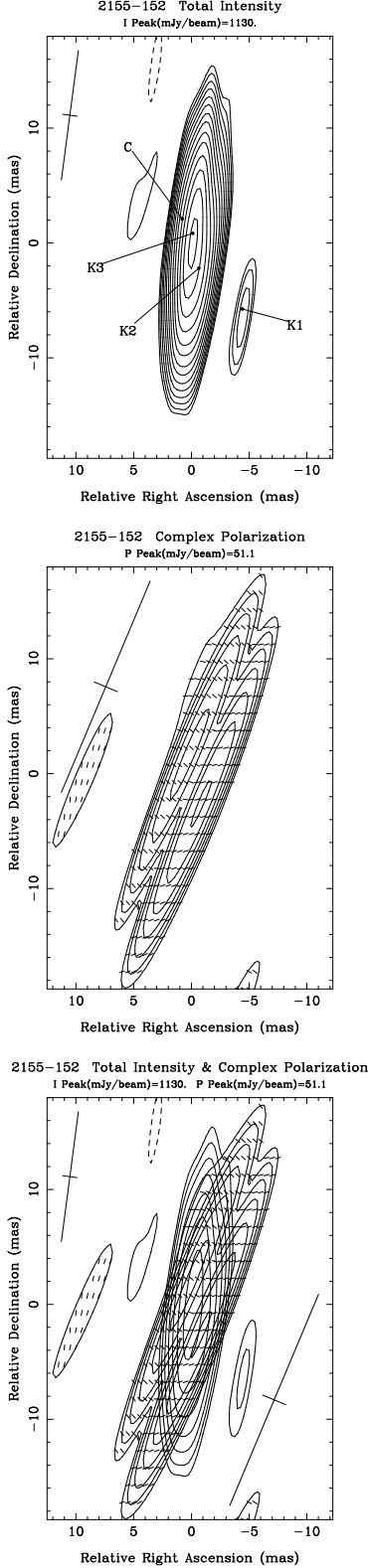


**Figure 9.** Total intensity VLBI hybrid map of 2155-152, with contours at  $-1.0, 1.0, 1.4, 2.0, 2.8, 4.0, 5.6, 8.0, 11, 16, 23, 32, 45, 64$ , and  $90\%$  of the peak brightness of  $1.22$  Jy/beam. (b) Linear polarization, with contours of polarized intensity at  $17, 24, 34, 48, 68, 96\%$  of the peak brightness of  $51$  mJy/beam, and  $\chi$  vectors superimposed. (c) Superposition of  $P$  image (heavy lines) over the  $I$  image, with every other  $I$  contour omitted.

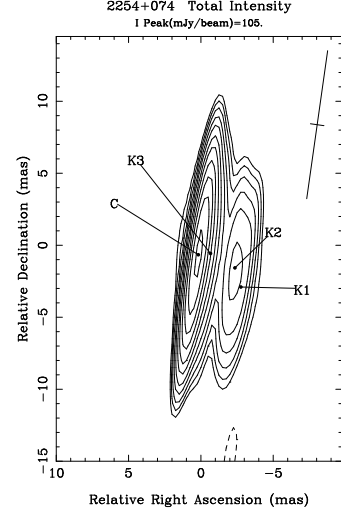


**Figure 10.** Total intensity VLBI hybrid map of 2254+074, with contours at  $-2.8, 2.8, 4.0, 5.6, 8.0, 11, 16, 23, 32, 45, 64$ , and  $90\%$  of the peak brightness of  $0.10$  Jy/beam.

mildly variable,  $m \sim 1.6\%$ , while  $\chi_{core}$  varied by about  $15^\circ$  over the course of the VLBI run, remaining roughly perpendicular to the direction of the VLBI jet (to within  $\sim 30^\circ$ ).

### 3.8 2150+173

This object is one of comparatively few in the sample whose spectra are so featureless that no redshift has been determined (Stickel et al. 1993b; Veron-Cetty & Veron 1993). The  $13$  and  $4$  cm VLBI images of Fey & Charlot (1997) show a prominent jet extending toward the northwest, which is also clearly visible in our images (Fig. 8). We detected polarization in the core and several jet components;  $\chi$  is predominantly transverse to the jet direction in both the core and jet.

### 3.9 2155-152

The redshift of this object is  $z = 0.67$  (Stickel et al. 1989). Its total intensity structure (Fig. 9) is somewhat unusual, with structure present on both sides of the brightest feature at the phase center. We believe that the strongest feature is a bright knot in the inner jet, and that the feature to the northeast of this component is the core; multi-frequency VLBA observations currently being analysed (Pushkarev et al., in prep.) confirm that the source has a core-jet structure with the jet extending toward the southwest. We detected polarization in the core to the northeast and the second jet component to the southwest. The polarized flux of the core varied during the VLBI run, while that of the jet component was constant (Gabuzda et al. 2000), with no detectable variability in  $\chi$  for either of these components. The map in Fig. 9b corresponds to one time subinterval considered in the variability analysis.  $\chi$  in the core is well aligned with the inner-jet direction, and is perpendicular to the jet direction in the SW component, suggesting that the dominant magnetic field in this part of the jet is longitudinal.

KUHR &amp; SCHMIDT BL LAC CORES

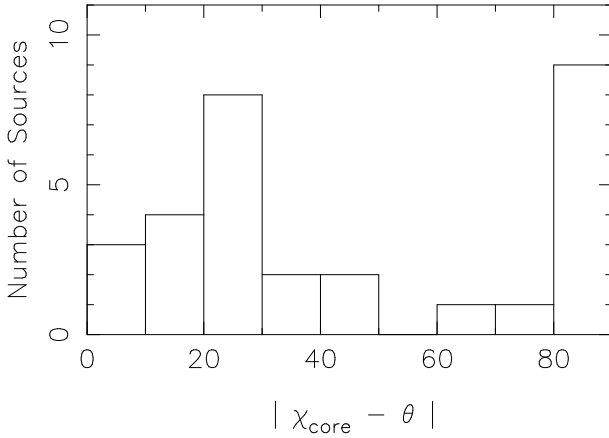


**Figure 11.** Distribution of offsets between the core  $\chi$  value (after correction for the integrated rotation measure) and the direction of the inner VLBI jet  $|\chi_{\text{core}} - \theta|$  for the 23 Kühr & Schmidt (1990) BL Lac objects for which such measurements are available. The distribution is clearly bimodal, with preferred values close to  $0^\circ$  and  $90^\circ$ .

### 3.10 2254+074

The host galaxy of this source, which has a redshift  $z = 0.19$  (Stickel et al. 1988), is clearly resolved in direct images (Stickel et al. 1993a; Falomo 1996). The BL Lac object is surrounded by a number of galaxies, one of which appears to be a physical companion (Stickel et al. 1993a). To our knowledge, no previous VLBI images are available. We detected three components in the VLBI jet (Fig. 10); the polarization of this source was not sufficiently strong to be detected.

## 4 VLBI PROPERTIES OF A COMPLETE SAMPLE OF 1-JY BL LACERTAE OBJECTS AT 6 CM

Having completed our first-epoch 6 cm polarization observations of all sources in the Kühr & Schmidt sample of BL Lacertae objects, we are now able to evaluate the VLBI properties of the sample as a whole. We summarize our results for the VLBI polarization properties of the sample sources in Table 4. The columns present (1) Source name (1950.0), (2) redshift  $z$ , (3) Epoch for the VLBI polarization observations, (4) total flux density on VLBI scales  $I_{\text{VLBI}}$ , (5) fraction of VLA core flux present on VLBI scales  $f_I$ , (6) total polarized flux density on VLBI scales  $p_{\text{VLBI}}$ , (7) fraction of VLA core polarized flux present on VLBI scales  $f_P$ , (8) position angle for the total polarization on VLBI scales  $\chi_{\text{VLBI}}$ , (9) position angle for the polarization of the VLA core  $\chi_{\text{VLA}}$ , (10) degree of polarization in the VLBI core  $m_c$ , (11) degree of polarization in the VLBI jet  $m_j$ , (12) offset between  $\chi_{\text{core}}$  and the jet direction  $|\theta - \chi_{\text{core}}|$ , (13) offset between  $\chi_{\text{jet}}$  and the jet direction  $|\theta - \chi_{\text{jet}}|$ , (14) integrated rotation measure RM, and (15) references. Separate rows are given for each epoch for which VLBI polarization data have been analyzed. When polarization was detected in more than one jet component at a given epoch, multiple entries separated by commas are given.

KUHR &amp; SCHMIDT BL LAC JETS

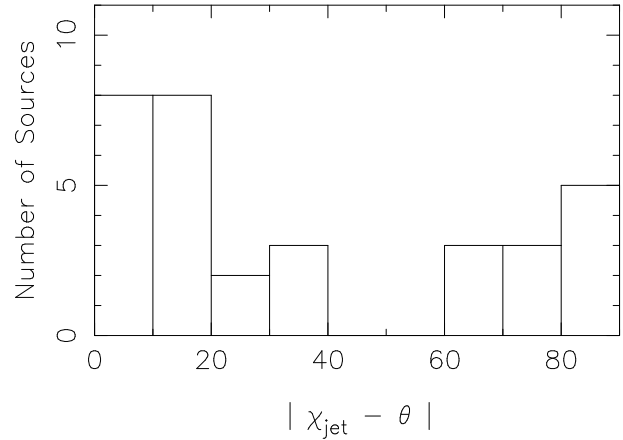


**Figure 12.** Distribution of offsets between the jet  $\chi$  value (after correction for the integrated rotation measure) and the local VLBI jet direction  $|\chi_{\text{jet}} - \theta|$  for the 20 Kühr & Schmidt (1990) BL Lac objects for which such measurements are available. The distribution shows a clear predominance of values close to  $0^\circ$ , with a weaker secondary peak near  $90^\circ$ .

The  $\chi_{\text{VLBI}}$  and  $\chi_{\text{VLA}}$  values are as observed, i.e., not corrected for Faraday rotation, but  $|\theta - \chi_{\text{core}}|$  and  $|\theta - \chi_{\text{jet}}|$  have both been determined after correction for the integrated rotation measure listed in column (16). The one exception is 0820+225, for which multi-frequency VLBI polarization observations have revealed a non-uniform distribution of the rotation measure on milliarcsecond scales (Gabuzda, Pushkarev & Garnich, in prep.); in this case, the values in columns (14) and (15) have been determined after correction for the local rotation measure in the VLBI jet.

### 4.1 Properties of the VLBI core polarization

Previous observations (Gabuzda et al. 1994b, 1999, and references therein) have indicated that the VLBI core polarizations of BL Lac objects are typically  $\sim 2 - 5\%$ . After completing our first-epoch polarization observations for the entire Kühr & Schmidt BL Lac sample, we have measurements of the VLBI core polarizations  $m_c$  for all but five of the 33 sample sources. These  $m_c$  values, collected in Table 4, with few exceptions range from 1.8 to 6.8%, demonstrating that the behaviour suggested by the earlier incomplete observations is, indeed, characteristic of BL Lac objects.

Another tendency indicated by the earlier observations was for the core polarization position angle  $\chi_{\text{core}}$  to be either aligned with or transverse to the direction of the inner 6 cm VLBI jet. We now have measurements of  $|\theta - \chi_{\text{core}}|$  for 24 of the 33 sample sources. The  $|\theta - \chi_{\text{core}}|$  values in Table 4 and in Fig. 11 clearly show this behaviour: in 16 cases,  $|\theta - \chi_{\text{core}}|$  is between  $0$  and  $30^\circ$ , and in 12 cases  $|\theta - \chi_{\text{core}}|$  is between  $60$  and  $90^\circ$ . This indicates that the  $|\theta - \chi_{\text{core}}|$  distribution for this  $\sim 73\%$  of the sample is bimodal, with the numbers of sources displaying either of the two preferred values for  $|\theta - \chi_{\text{core}}|$  being roughly equal. It appears that the peak at small misalignments may be offset from  $0^\circ$ ; the origin of this behaviour is not clear, though it could be associated with

uncertainty in the jet direction on scales slightly smaller than the resolution of our 6 cm global observations.

#### 4.2 Characteristics of the jet magnetic fields

Earlier observations indicated a tendency for  $\chi$  in the VLBI jets of BL Lacertae objects to be parallel to the local jet direction, which has usually been interpreted as evidence for the presence of relativistic plane shocks. We now have measurements of  $|\theta - \chi_{jet}|$  for 25 of the 33 sample sources. The  $|\theta - \chi_{jet}|$  values in Table 4 and in Fig. 12 clearly show a predominance of sources with  $\chi_{jet}$  and  $\theta$  aligned to within  $\sim 30^\circ$  ( $\sim 60\%$ ). At the same time, the histogram shows a weaker secondary peak of sources with  $|\theta - \chi_{jet}|$  near  $90^\circ$ . Thus, it is clear that, as hinted by previous observations (Gabuzda et al. 1999 and references therein), a sizeable fraction ( $\sim 30\%$ ) of sources in the Kühr & Schmidt (1990) sample of BL Lacertae objects have longitudinal magnetic fields in their VLBI jets. At this time, it is not clear how jet components with transverse and longitudinal magnetic fields physically differ; multi-frequency VLBA polarization observations for all the sample sources currently under analysis will hopefully help elucidate this question in the near future.

In the remaining sources,  $\chi_{jet}$  bears no obvious relation to  $\theta$ , possibly due to the presence of Faraday rotation with substantially different values than suggested by the integrated rotation measures. Multi-frequency polarization observations currently being analyzed should shed light on this issue.

#### 4.3 Superluminal motion

Among the sources for which images are presented and analysed here, to our knowledge, previous VLBI images at 6 cm or nearby wavelengths are available for five of them: 0003–066, 0823+033, 1732+389, 2131–021, and 2150+173. 1732+389 was observed at epoch 1990.18 as part of the 6 cm Caltech–Jodrell Bank Survey (Xu et al. 1995). The other four sources were observed at 4 cm by Fey & Charlot (1997; hereafter FC).

In their 6-cm image of 1732+389, Xu et al. (1995) detected a single jet component at  $r = 0.54$  mas. It is natural to tentatively identify this feature with K3 in Table 3. Our second-epoch observations at epoch 1995.41 support this identification, and indicate that the apparent proper motion of this feature is 0.24 mas/yr, which corresponds to an apparent speed  $\beta_{app}h = 6.5$  (Pushkarev & Gabuzda 1999a). The feature K2 is also present in our 1995.41 image; a comparison suggests a tentative proper motion of 0.61 mas/yr, corresponding to an apparent speed  $\beta_{app}h = 16.5$  (Pushkarev & Gabuzda 1999a).

FC obtained images of a large number of compact extragalactic radio sources at 13 and 3.6 cm. We will be interested primarily in the 3.6 cm images, since they have higher resolution and the observing wavelength is closer to that for our data. We must be aware of possible small frequency-dependent shifts in the apparent separations of jet components from the core when comparing these 3.6 cm images with our own 6 cm images. However, these two wavelengths are close enough that we would not expect such shifts to be

Speeds for 16 Kuhr & Schmidt BL Lacs

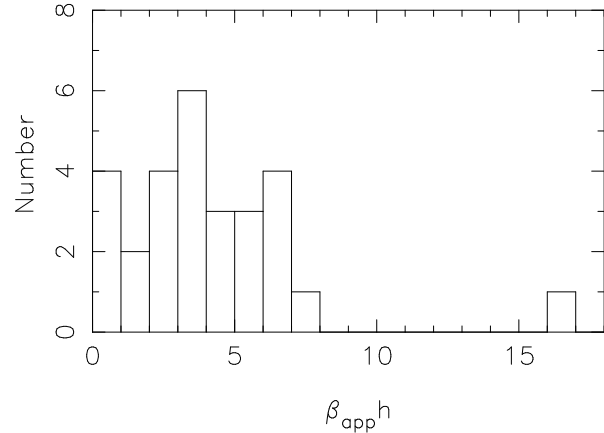


**Figure 13.** Distribution of apparent superluminal speeds for the sixteen Kühr & Schmidt (1990) BL Lac objects with redshifts for which component speed estimates are available. With the exception of the one very high speed of  $\beta_{app}h = 16.6$ , the range of apparent speeds is relatively small, and extends to considerably lower speeds than observed in core-dominated quasars (Fig. 14).

significant in most cases, so that the 3.6 cm data of FC can be used to derive at least tentative estimates of the structural changes in the sources observed in both projects. Below, we will refer to the 3.6 cm images of FC unless explicitly stated otherwise.

FC’s 3.6 cm observations of 0003–066 were less than five months after our first-epoch observations. There is a reasonably close correspondance between the jet structures detected in the two observations, but the interval between them is too short to reliably identify systematic proper motions. Most features appear to be stationary to within the errors. We therefore postpone estimation of the apparent speeds in the VLBI jet of this source until the results of our second-epoch observations become available.

FC detected only a single jet component in 0823+033 at epoch 1995.28, at  $r = 1.9$  mas. There are no components in our image near this position. If we assume expansion of the source structure with time, the simplest joint interpretation of the two images is that the feature detected by FC is K3 in Table 3. In this case, its tentative proper motion is 0.39 mas/yr, which corresponds to an apparent speed  $\beta_{app}h = 6.9$ .

Two jet components were detected by FC in 2131–021: one at  $r = 0.5$  mas in  $\theta = 107^\circ$  and another at  $r = 1.6$  mas in  $\theta = 75^\circ$ . A comparison with the model for this source in Table 3 shows that these positions nearly coincide with those for our components K5 and K4. In both cases, the positions of these features in the two images agree to within the errors. Thus, the simplest joint interpretation of the two images is that K4 and K5 were stationary from epoch 1992.23 to epoch 1995.78.

There is a very good correspondance between the structures in our image of 2150+173 and the image of FC, in which features were detected at  $r = 0.8, 1.9, 4.0$ , and 6.9 mas. It seems likely that these four components should be identified with K5, K4, K3, and K2 in Table 3. In this case, the implied proper motions for these features are

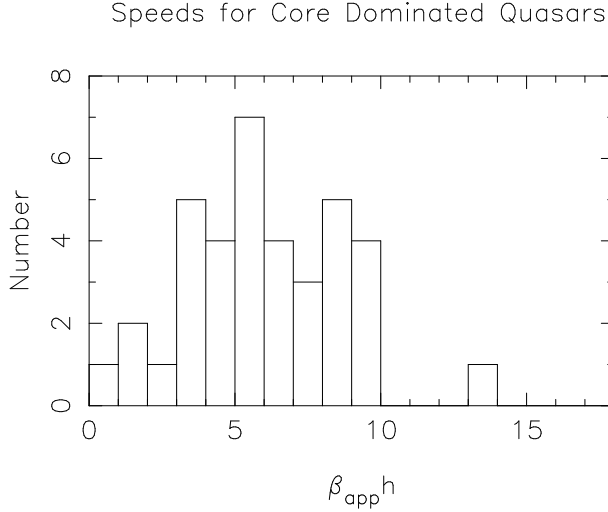


**Figure 14.** Distribution of apparent superluminal speeds for nineteen core-dominated quasars from Vermeulen & Cohen (1994). The distribution extends to appreciably higher speeds than the distribution for the Kühn & Schmidt BL Lacertae objects shown in Fig. 13.

$\mu = 0.01, 0.11, 0.27$ , and  $0.32$  mas/yr, respectively; we can see that this suggests acceleration with distance from the core, but further observations are required to test this hypothesis. Unfortunately, the redshift of this source is unknown, so that it is not possible to directly translate these proper motions into apparent speeds.

Finally, we have one more tentative speed to report here. At the time of the analysis for our first-epoch 6 cm observations of 0138–097 (Gabuzda et al. 1999), we were not aware that FC had also observed this source at 3.6 cm. They detected a single jet component 1.9 mas from the core. If this feature should be identified with K2 from Gabuzda et al. (1999), this implies a proper motion of  $0.35$  mas/yr, which corresponds to a tentative apparent speed  $\beta_{app}h = 5.53$ .

Our observations have substantially increased the number of objects in the Kühn & Schmidt sample with at least tentative (two-epoch) speed estimates. Such estimates are now available for 16 of the 33 sample sources, and are summarized in Table 5. The histogram in Figure 13 shows the distribution of superluminal speeds in these 16 objects. When making this histogram, we included more than one entry per source only if appreciably different speeds were observed for different components (i.e., only if the speeds fell in different bins). We can see that there is a concentration toward relatively low values, and the apparent speeds are fairly uniformly distributed in the range from  $0 - 7\beta_{app}h$ , with a possible weak peak near  $\sim 4$ . We see no evidence from this distribution that the typical jet Lorentz factors exceed  $\gamma \sim 5 - 6$ . There is some evidence for the occurrence of higher superluminal speeds in some BL Lacertae objects on the smaller scales probed by higher-frequency observations (e.g., Marscher & Marchenko 1998); it remains unclear whether the jets of BL Lacertae objects in general tend to display higher superluminal speeds on smaller scales.

Figure 14 shows the distribution of superluminal speeds for components in 19 core dominated quasars taken from Vermeulen & Cohen (1994). Here, as for the distribution in

**Table 5.** COMPONENT SPEEDS IN KÜHN & SCHMIDT BL LACERTAE OBJECTS

Source	$z$	N	$\mu$ (mas/yr)	$\beta_{app}h$	Ref.
0138–097	0.44	2	0.35	5.5	12
0454+844	0.11	5	0.14	0.6	1,3
0716+714	...	4	0.07	...	1,8
...	...	2	0.11	...	8
0735+178	$> 0.42$	4	0.48	7.4	5,6
		4	0.33	5.0	6
		3	0.28	4.2	6
0823+033	0.51	2	0.39	6.9	12
0828+493	0.55	2	0.34	6.3	9
0851+202	0.31	3	0.20	2.4	2
		3	0.27	3.2	2
0954+658	0.37	2	0.37	5.2	7
		2	0.44	6.2	7
1418+546	0.15	3	0.56	3.6	9,10
		2	0.08	0.5	9,10
1652+398	0.03	3	0.27	0.4	7
		2	0.55	0.8	7
1732+389	0.97	3	0.24	6.5	10,12
		2	0.61	16.6	10,12
1749+701	0.77	3	0.14	3.2	7
		3	0.08	2.0	7
		2	0.09	2.1	7
1803+784	0.68	2	0.08	1.8	7
1823+568	0.34	3	0.18	3.8	7
		2	0.20	4.3	7
2007+777	0.34	5	0.22	2.9	1,7
2200+420	0.07	4	1.14	3.7	4
		5	1.12	3.6	4
		4	1.12	3.6	4
		2	1.00	3.3	4
2150+173	...	2	0.01	...	12
		2	0.11	...	12
		2	0.28	...	12
		2	0.34	...	12
2254+074	0.19	2	0.46	3.7	11,12
		2	0.30	2.4	11,12
		2	0.55	4.3	11,12

Refs: 1 = Witzel et al. 1988; 2 = Gabuzda, Wardle & Roberts 1989a; 3 = Gabuzda et al. 1989; 4 = Mutel et al. 1990; 5 = Bååth & Zhang 1991; 6 = Gabuzda et al. 1994a; 7 = Gabuzda et al. 1994b; 8 = Gabuzda et al. 1998; 9 = Gabuzda et al. 1999; 10 = Pushkarev & Gabuzda 1999a; 11 = Pushkarev & Gabuzda 1999b; 12 = This paper.

Fig. 13, we have not plotted more than one entry per source per bin. We can see that the quasar speed distribution has fewer values below  $\sim 3$  and appreciably more values exceeding  $\sim 7$  than the BL Lac distribution. The overall centroid of the distribution is shifted toward higher speeds: the median and average speeds for the BL Lacertae objects are both  $3.7$ , while the corresponding values for the quasars are both  $5.8$ . A Kolmogorov–Smirnov test indicates that the probability that the two distributions are the same is less than 1%. This confirms previous evidence that the superluminal speeds in BL Lac objects are systematically lower than those observed in core-dominated quasars (Gabuzda et al. 1994b; Britzen et al. 1999).

## 5 CONCLUSION

This paper completes analysis of our first-epoch observations of all sources in the complete sample of BL Lacertae objects defined by Kühr & Schmidt (1990). Certain tendencies were present even in the earliest VLBI polarization observations of BL Lac objects; however, without systematic observations of a complete sample of objects, it was not possible to say whether these properties were relevant for radio-loud BL Lac objects in general, or only to a handful of the best studied sources. On the whole, our analysis of the complete sample has confirmed the results of these early observations. However, it is also clear that the behaviour shown by the sample sources is not entirely uniform. We summarize our results below.

The VLBI core polarizations of BL Lacertae objects are appreciable, with values typically ranging from  $\sim 2 - 7\%$ , and occasionally reaching values as high as  $\sim 10\%$ . Gabuzda et al. (1994b) suggested that these relatively high values reflected the dominant contribution of newly emerging jet components. In the case of one source in the sample – 1803+784 – 6 cm space VLBI polarization observations directly showed that the polarized flux was dominated by a compact component in the inner VLBI jet, which was unresolved from the core in ground-based observations (Gabuzda 1999).

The 6 cm VLBI core polarizations of quasars are much lower, typically  $\leq 2\%$  (Cawthorne et al. 1993). This suggests that either the cores of quasars are depolarized (see, e.g., Taylor 1998, 2000), or that they are considerably less likely to be dominated by emission from compact new jet components. If the VLBI cores of quasars are depolarized, we expect that the observed degrees of polarization of the cores of quasars and BL Lac objects will become more similar at higher frequencies; thus far, there is no clear evidence for this, but more systematic studies are required.

Thus, it remains a possibility that the VLBI core polarizations of BL Lac objects are more often dominated by the contribution of emerging jet components than are the VLBI core polarizations of quasars. The origin of this systematic difference is not obvious. One possibility is that the birth rate for new jet components is higher in BL Lacertae objects than in quasars, increasing the probability of observing a BL Lac object core harbouring new jet components. There is some evidence from the University of Michigan monitoring database that outbursts in BL Lacertae objects may be more frequent and well resolved than those in quasars, suggesting that BL Lac objects may generate new components more frequently (M. Aller, private communication). Since the superluminal speeds observed in BL Lacertae objects are, on average, slower than those in quasars, it may be that the jet components of BL Lacertae objects spend more time in the unresolved core region before becoming detectable as distinct jet knots. Another possibility is that highly-polarized jet components close to the core are often long-lived stationary components whose polarization blends with the true core polarization. Quasi-simultaneous multi-frequency VLBA observations for all sources in the Kühr & Schmidt sample currently being analyzed should help distinguish between these various possibilities.

One of the striking tendencies noted in the earliest VLBI polarization results was for the jets of BL Lacertae

objects to have transverse magnetic fields. Our first-epoch images for the complete Kühr & Schmidt sample confirm that this is the predominant behaviour for the sample as a whole: among the 25 sources in which jet polarization was detected, some 60–70% have transverse magnetic fields. At the same time, a sizeable minority of about 30% have longitudinal jet magnetic fields. Thus far, transverse magnetic fields have usually been interpreted as manifestations of relativistic shocks in the VLBI jets of these sources, while longitudinal fields have been taken to reflect the presence of shear between the jet and the surrounding medium. In this picture, the common presence of transverse magnetic fields reflects the existence of conditions favorable for the formation of transverse shocks; the jet components with dominant longitudinal fields would be those in which shocks did not form, or did form but were dominated by the effect of shear.

Though it seems likely that many individual, compact, highly-polarized features with transverse magnetic fields are associated with shocks, this does not necessarily imply that *all* the observed transverse jet fields should be identified with shock components. Another possibility is that, in at least some cases, we are detecting the toroidal component of an intrinsic helical jet magnetic field (see, e.g., Gabuzda 1999). If the dominant magnetic field in the jet is helical, the net observed field can be either transverse or longitudinal, depending on the pitch angle of the field and the viewing angle, though it is more likely that the net observed field will be transverse. In addition, a longitudinal field component could develop due to interaction between the edges of the jet and the surrounding medium (e.g. Aaron 1998, Laing et al. 1999, Aloy et al. 2000). Thus, it could be that the dominant magnetic-field component in the VLBI jets of BL Lacertae objects is characteristically toroidal. This could be consistent with the fact that the observed jet magnetic fields are most often transverse, but occasionally longitudinal.

The characteristically modest superluminal speeds observed in the Kühr & Schmidt sources suggest that BL Lacertae objects differ from quasars in either the characteristic angles of their jets to the line of sight, or the characteristic intrinsic velocities of components in their jets, or both. The observed apparent speed for a VLBI feature has a peak for motion at an angle to the line of sight of about  $\theta \sim 1/\gamma$ , where  $\gamma$  is the Lorentz factor of the motion. Therefore, if the intrinsic velocities in the two types of sources were essentially the same, the BL Lacertae objects could, in principle, have smaller apparent velocities if their jets were significantly further from or nearer to the line of sight than the jets in quasars. Since BL Lacertae objects are obviously highly beamed sources (Kollgaard 1994, for example), it is not reasonable to suppose that their jets could typically be at significantly larger angles to the line of sight than those in quasars. On the other hand, if their jets were significantly *closer* to the line of sight than quasar jets, we would expect BL Lacertae objects to be significantly more highly beamed than quasars, and there is no evidence for this (Ghisellini et al. 1993). Thus, the most straightforward interpretation of the more modest superluminal speeds observed in the VLBI jets of BL Lacertae objects compared to quasars is that the intrinsic velocities in the BL Lac jets are lower. This seems quite natural in the context of unified schemes linking BL Lacertae objects with FR I and quasars with FR II radio galaxies.

## 6 ACKNOWLEDGEMENTS

This work was supported by an American Astronomical Society Henri Chretien International Research Grant and Small Grant (DCG). ABP acknowledges support from the Russian Foundation for Basic Research. DCG acknowledges support from the European Commission under the IHP Programme (ARI) contract No. HPRI-CT-1999-00045. We would like to thank R. M. Campbell for useful discussions of some aspects of our analysis. We also thank the staff at the participating observatories and correlation facilities who made these observations possible. This research has made use of data from the University of Michigan Radio Astronomy Observatory, which is supported by the National Science Foundation and by funds from the University of Michigan.

## REFERENCES

- Aaron S., 1999, in *The BL Lac Phenomenon*, ASP Conf. Ser., 159, 427.
- Aloy M.-A., Gómez J.-L., Ibañez J.-M., Martí J.-M., & Müller E., 2000, ApJ, 528, L85.
- Angel J.R.P., Stockman H.S., 1980, ARA&A, 8, 321.
- Bääth L.B. & Zhang F.J., 1991, A&A, 243, 328.
- Britzen S., Vermeulen R.C., Taylor G.B., Readhead C.S., Pearson T.J., Henstock D.R., & Wilkinson P.N., 1999, in *The BL Lac Phenomenon*, ASP Conf. Ser., 159, 431.
- Browne I. W. A., 1983, MNRAS, 204, 23P.
- Cawthorne T.V., Wardle J.F.C., Roberts D.H., Gabuzda D.C., & Brown, L.F., 1993, ApJ, 416, 496.
- Cornwell T.J., Wilkinson P.N., 1981, MNRAS, 196, 1067.
- Drinkwater M.J., Webster, R.L., Francis, P.J., Condon, J.J., Ellison S.L., Jauncey D.L., Lovell J., Peterson B.A., & Savage A., 1997, MNRAS, 284, 85.
- Falomo, R. 1996, MNRAS, 283, 241.
- Fey A.L. & Charlot P., 1997, ApJS, 111, 95.
- Fossati, G., Celotti, A., Ghisellini, G., & Maraschi, L. 1997, MNRAS, 289, 136.
- Gabuzda D.C. 1999, New Astronomy Reviews, 43, 691.
- Gabuzda D.C. & Cawthorne T.V. 1996, MNRAS, 283, 759.
- Gabuzda D.C., Cawthorne T.V., Roberts D.H., Wardle J.F.C., 1989, ApJ, 347, 701.
- Gabuzda D.C., Cawthorne T.V., Roberts D.H., Wardle J.F.C., 1992, ApJ, 388, 40.
- Gabuzda D.C., Kochenov P.Yu., & Cawthorne T.V. 2000, MNRAS, submitted.
- Gabuzda D.C., Mullan C.M., Cawthorne T.V., Wardle J.F.C., Roberts D.H., 1994b, ApJ, 435, 140.
- Gabuzda D.C., Pushkarev A.B., & Cawthorne T.V., 1999, MNRAS, 307, 725.
- Gabuzda D.C., Sitko, M.L., Smith, P.S., 1996, AJ, 112, 1877.
- Gabuzda D.C., Wardle J.F.C., & Roberts D.H., 1989a, ApJ, 336, L59.
- Gabuzda D.C., Wardle J.F.C., & Roberts D.H., 1989b, ApJ, 338, 743.
- Gabuzda D.C., Wardle J.F.C., Roberts D.H., Aller M.F., & Aller H.D., 1994a, ApJ, 435, 128.
- Ghisellini G., Padovani P., Celotti A., & Maraschi L., 1993, ApJ, 407, 65.
- Giommi, P. & Padovani, P. 1994, MNRAS, 268, P51.
- Hughes P.A., Aller H.D., Aller M.F., 1989, ApJ, 341, 68.
- Kellermann K. I., Vermeulen R. C., Zensus J. A., & Cohen M. H., 1998, AJ, 115, 1295.
- Kollgaard R.I., 1994, Vistas in Astronomy, 38, 29.
- Kühr, H. & Schmidt, G.D. 1990, AJ, 90, 1.
- Laing R., 1980, MNRAS, 193, 439.
- Laing R.A., Parma P., de Ruiter H.R., & Fanti R., 1999, MNRAS, 306, 513.
- Lister M.L., Marscher A.P., & Gear W.K., 1998, ApJ, 504, 702.
- Maraschi, L., Ghisellini, G., Tanzi, E. G., & Treves, A. 1986, ApJ, 310, 325.
- Marscher A.P. & Marchenko S.G., 1999, in *The BL Lac Phenomenon*, ASP Conf. Ser., 159, 417.
- Miller J.S., 1981, PASP, 93, 681.
- Mutel R.L., Su Bumei, Bucciferro R.R., & Phillips R.B., 1990, ApJ, 352, 81.
- Padovani, P. & Giommi, P. 1995, ApJ, 444, 567.
- Pushkarev, A. B. & Gabuzda, D. C. 1999a, in *The BL Lac Phenomenon*, ASP Conf. Ser., 159, 458.
- Pushkarev, A. B. & Gabuzda, D. C. 1999b, New Astronomy Reviews, 43, 695.
- Roberts D.H., Gabuzda D.C., Wardle J.F.C., 1987, ApJ, 323, 536.
- Roberts D.H., Wardle J.F.C., Brown L.F., 1994, ApJ, 427, 718.
- Rudnick L., Jones T.W., 1983, AJ, 88, 518.
- Rusk R., 1988, Ph.D. thesis, University of Toronto.
- Stickel M., Fried J.W., Kühr H., 1988, A&A, 191, 16.
- Stickel M., Fried J.W., Kühr H., 1989, A&AS, 80, 113.
- Stickel M., Fried J.W., Kühr H., 1993a, A&AS, 98, 393.
- Stickel M., Kühr H., & Fried J.W., 1993b, A&AS, 97, 393.
- Stoeck, J.T., Liebert, J., Schmidt, G., Gioia, I.M., Maccaro, T., Schild, R.E., Maccagni, D., & Arp, H. C. 1985, ApJ, 298, 619.
- Vermeulen, R.C. & Cohen, M.H. 1994, ApJ, 430, 467.
- Veron-Cetty M.P. & Veron P., 1993, A&AS, 100, 521.
- Wardle J. F. C., Moore R. L., & Angel, J. R. P., 1984, ApJ, 279, 93.
- Wilkes, B.J., 1986, MNRAS, 218, 331.
- Wills, D. & Wills, B.J., 1976, ApJS, 31, 143.
- Witzel A., Schalinski C.J., Johnston K.J., Biermann P.L., Krichbaum T.P., Hummel C.A., & Eckart A., 1988, A&A, 206, 245.
- Wurtz R., Stoeck, J.T., & Yee, H.K.C., 1996, ApJS, 103, 109.
- Xu, W., Readhead, A.C.S., & Pearson, T.J. 1995, ApJS, 99, 297.